Int. J. Heat Mass Transfer. Vol. 29, No. 9, pp. 1359–1369, 1986
Printed in Great Britain

0017–9310/86 $3.00 + 0.00
Pergamon Journals Ltd.

Numerical simulation of melting of ice around a horizontal cylinder

C. J. HO and S. CHEN
Department of Mechanical Engineering, National Cheng Kung University, Tainan, Taiwan, R.O.C.

(*Received* 12 *September* 1985 *and in final form* 21 *January* 1986)

Abstract—The problem of outward melting of ice around a horizontal isothermal cylinder is considered. A numerical model in which natural convection induced in the molten water encompassing density inversion is taken into consideration has been developed. Via finite-difference solution of the melting model, numerical simulation of melting of ice has been performed for the cylinder surface temperature $T_i = 4$, 6, 8, 9 and 10°C with cylinder radius of 25.4 mm. The results of the present simulation were found qualitatively valid when compared with the existing experimental data.

INTRODUCTION

UNDERSTANDING the solid–liquid phase change (melting/solidification) heat transfer characteristics is of fundamental importance in a wide range of naturally occurring processes and engineering applications such as the formation of ice on a lake or river, the freezing of water pipes, metal processing, freezing of foodstuffs, thermal control of space craft, and thermal energy storage system. In recent years, the impetus for considerable attention on the heat transfer problems associated with melting and solidification has been heightened by the proposed feasible applications of phase change processes for thermal energy storage system.

Experimental results [1–4] have provided conclusive evidence that during the melting process around a horizontal heated cylinder the natural convective motion induced in the melt plays a dominant role except in the earliest stage of the phase change process. These experimental investigations lead to the conclusion that natural convection has to be taken into account in the analysis for predicting the melting phenomena. Phase-change heat transfer problems in the presence of natural convection of melt exhibit considerable difficulty and complexity in the analytical studies due to the fact that the solid–liquid interface movement is a transient phenomena as well as an unknown of the problem. A comprehensive survey of the recent literature on the analysis of solid–liquid phase change problems is given by Viskanta [5]. Among various analysis techniques, numerical methods appear to be the most viable approach. Numerical simulations of melting process around a heated single tube or cylinder have been conducted by Yao *et al.* [6] and Rieger *et al.* [7]. These analyses show that as a result of the recirculation induced in the melt and thermal plume activity, a "pear-shape" solid–liquid interface is formed, which is in good accord with the earlier experimental results [1–4].

Recently, the influence of density inversion on the melting of ice around a horizontal heated cylinder was studied experimentally consecutively by Herrmann *et al.* [8] and White [9]. Their findings indicate that due to the density anomaly the melt shape resembles an upside-down pear shape for cylinder temperature below 8°C and an upright pear for cylinder temperature above 8°C. Moreover, White [9] has successfully visualized the natural convection flow patterns in the molten water during the melting process.

The primary objective of this paper is to simulate numerically the heat transfer process during the outward melting of ice around a horizontal isothermal cylinder. Natural convection as well as the density anomaly of the water are included in the melting model. Comparisons are made between the predicted results and the existing experimental data and the agreement appears to be reasonably good.

PHYSICAL PROBLEM AND MATHEMATICAL FORMULATION

Figure 1 illustrates schematically the physical problem of ice undergoing outward melting process around a horizontal isothermal heated cylinder of radius r_i. Initially ice is at its fusion temperature T_f. Melting is started by suddenly raising the temperature of the cylinder to a specified temperature $T_i > T_f$. Mathematically the process of solid–liquid phase change is characterized by the existence of time dependent moving phase change boundary, which is described by a function of angular position ϕ^+ and time t, $S(\phi^+, t)$.

In the development of a convenient mathematical formulation for the melting process in the presence of natural convection of the melt, the following idealization are assumed:

(1) Fluid motion of water is two-dimensional laminar incompressible flow.
(2) The physical properties of water/ice are temperature independent except the density, for

NOMENCLATURE

C_p	specific heat
F_0	Fourier number, $= \alpha t/r_i^2$
g	gravitational acceleration
Δh_f	heat of fusion
K	thermal conductivity
Nu	Nusselt number
Pr	Prandtl number
q	temperature index
r	radial coordinate
r_i	radius of cylinder
rsp	temperature coefficient
Ra	Rayleigh number, $rsp \cdot a \cdot r_i^3 \cdot (T_i - T_f)^q / \{\alpha \cdot \nu \cdot (1 - rsp) \lvert T_{mean} - T_m \rvert^q\}$
S	radial position of ice interface
Ste	Stefan number, $C_p(T_i - T_f)/\Delta h_f$
t	time
T	temperature
V^*	melt volume ratio.

Greek symbols

α	thermal diffusivity
η	transformation variable
θ	dimensionless temperature, $(T - T_f)/(T_i - T_f)$
ν	kinematic viscosity
τ	dimensionless time, $Ste \cdot F_0$
ϕ^+	angular coordinate
ϕ	dimensionless angular coordinate, ϕ^+/π
ψ^+	stream-function
ψ	dimensionless stream-function
ω^+	vorticity
ω	dimensionless vorticity
∇^2	Laplace operator
$\hat{\nabla}^2$	Laplace operator in transformed plane.

Subscripts

f	fusion
i	cylinder surface
m	physical properties of water at 4.029325°C
mean	physical properties of water at film temperature
s	ice interface.

which the density variation in the water are considered insofar as they contribute to buoyancy but are otherwise neglected.

(3) The volume change associated with phase change and the viscous dissipation are neglected.

(4) The water is a Newtonian fluid.

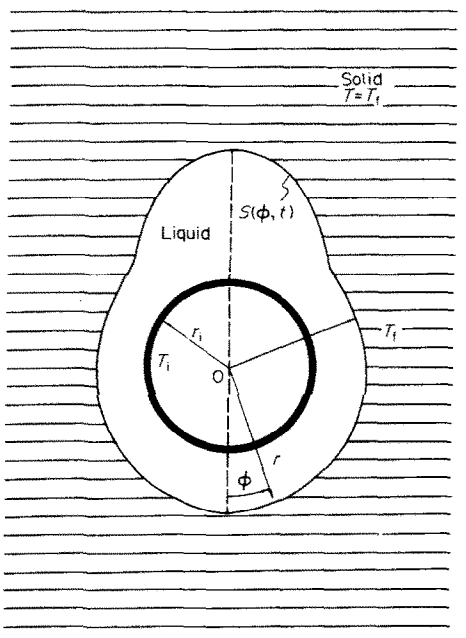

FIG. 1. Schematic representation of the physical problem.

To describe the nonlinear variation of density with temperature for water in the range of 0 to 20°C, the relation given by Gebhart and Mollendorf [10]

$$\rho = \rho_m(1 - rsp|T - T_m|^q), \tag{1}$$

where

$$\rho_m = 999.9720\,\text{kg/m}^3,$$

$$rsp = 9.297173 \times 10^{-6}/°\text{C}$$

$$T_m = 4.029325°\text{C}, \quad q = 1.894816$$

is used.

With the foregoing, the fluid motion and temperature distribution in the water during melting of ice are governed by the normalized partial differential equations in vorticity–stream-function–temperature formulation as follows.

Vorticity equation:

$$\frac{\partial \omega}{\partial F_0} + \frac{1}{\pi r}\left(\frac{\partial \psi}{\partial \phi}\frac{\partial \omega}{\partial r} - \frac{\partial \psi}{\partial r}\frac{\partial \omega}{\partial \phi}\right) = Pr\nabla^2\omega + Pr \cdot Ra \cdot \left[\sin(\pi\phi)\frac{\partial}{\partial r}|\theta - \theta_m|^q + \frac{\cos(\pi\phi)}{\pi r}\frac{\partial}{\partial \phi}|\theta - \theta_m|^q\right]. \tag{2}$$

Stream-function equation:

$$\nabla\psi = -\omega. \tag{3}$$

Energy equation:

$$\frac{\partial \theta}{\partial F_0} + \frac{1}{\pi r}\left(\frac{\partial \psi}{\partial \phi}\frac{\partial \theta}{\partial r} - \frac{\partial \psi}{\partial r}\frac{\partial \theta}{\partial \phi}\right) = \nabla^2\theta \tag{4}$$

where

$$\nabla^2 \equiv \frac{\partial^2}{\partial r^2} + \frac{1}{r}\frac{\partial}{\partial r} + \frac{1}{(\pi r)^2}\frac{\partial^2}{\partial \phi^2}.$$

For complete mathematical formulation, the foregoing set of equations (2–4) are subjected to the following boundary conditions:

$$\phi = 0 \quad \text{or} \quad 1; \quad \frac{\partial \theta}{\partial \phi} = \psi = \omega = 0 \quad \text{(Symmetry lines)}$$

$$r = 1; \quad \theta = 1, \quad \psi = \frac{\partial \psi}{\partial r} = 0$$

$$r = S; \quad \theta = 0, \quad \psi = \frac{\partial \psi}{\partial r} = 0 \tag{5}$$

and moreover energy balance at the solid–liquid interface gives

$$\frac{\partial S}{\partial F_0} = -Ste\left(1 + \left(\frac{1}{\pi S}\frac{\partial S}{\partial \phi}\right)^2\right)\frac{\partial \theta}{\partial r}. \tag{6}$$

In view of the fact that the physical domain of the above set of equations (2)–(6) is not known *a priori*, but is irregular and time-dependent due to the existence of the moving phase interface, a coordinate transformation is employed to immobilize this moving irregular solid–liquid interface and thus a more tractable computational domain for numerical solution of the problem can be obtained. For the present study, the following coordinate transformation is adopted.

$$\eta = \frac{r-1}{S-1}. \tag{7}$$

Consequently, the molten water region is then mapped into a regular domain characterized by $0 \leqslant \eta \leqslant 1$ for all ϕ during any time interval and the solid–liquid interface in the transformed plane is stationary and defined by $\eta = 1$. And the transformed version of the governing equations becomes:

Vorticity equations:

$$\frac{\partial \theta}{\partial F_0} + \frac{\partial \eta}{\partial F_0}\frac{\partial \omega}{\partial \eta} + \frac{1}{\pi r}\frac{\partial \eta}{\partial r}\left(\frac{\partial \psi}{\partial \phi}\frac{\partial \omega}{\partial \eta} - \frac{\partial \psi}{\partial \eta}\frac{\partial \omega}{\partial \phi}\right)$$
$$= Pr\hat{\nabla}^2\omega + PrRa\left[\sin(\pi\phi)\frac{\partial \eta}{\partial r}\frac{\partial}{\partial \eta}|\theta - \theta_m|^q + \frac{\cos(\pi\phi)}{\pi r}\left(\frac{\partial}{\partial \phi}|\theta-\theta_m|^q + \frac{\partial \eta}{\partial \phi}\frac{\partial}{\partial \eta}|\theta-\theta_m|^q\right)\right]. \tag{8}$$

Stream-function equation:

$$\hat{\nabla}^2\psi = -\omega. \tag{9}$$

Energy equation:

$$\frac{\partial \theta}{\partial F_0} + \frac{\partial \eta}{\partial F_0}\frac{\partial \theta}{\partial \eta} + \frac{1}{\pi r}\frac{\partial \eta}{\partial r}\left(\frac{\partial \psi}{\partial \phi}\frac{\partial \theta}{\partial \eta} - \frac{\partial \psi}{\partial \eta}\frac{\partial \theta}{\partial \phi}\right) = \hat{\nabla}^2\theta, \tag{10}$$

where

$$\hat{\nabla}^2 \equiv \left[\left(\frac{\partial \eta}{\partial r}\right)^2 - \left(\frac{1}{\pi r}\frac{\partial \eta}{\partial \phi}\right)^2\right]\frac{\partial^2}{\partial \eta^2} + \frac{2}{(\pi r)^2}\frac{\partial \eta}{\partial \phi}\frac{\partial^2}{\partial \eta\,\partial \phi} + \frac{1}{(\pi r)^2}\frac{\partial^2}{\partial \phi^2} + \left[\frac{1}{r}\frac{\partial \eta}{\partial r} + \frac{1}{(\pi r)^2}\frac{\partial^2 \eta}{\partial \phi^2}\right]\frac{\partial}{\partial \eta} \tag{11}$$

$$\frac{\partial \eta}{\partial F_0} = -\frac{\eta}{(S-1)}\frac{\partial S}{\partial F_0} \tag{12}$$

$$\frac{\partial \eta}{\partial r} = \frac{1}{S-1} \tag{13}$$

$$\frac{\partial \eta}{\partial \phi} = -\frac{\eta}{S-1}\frac{\partial S}{\partial \phi} \tag{14}$$

$$\frac{\partial^2 \eta}{\partial \phi^2} = \frac{-1}{S-1}\left(\eta\frac{\partial^2 S}{\partial \phi^2} + 2\frac{\partial \eta}{\partial \phi}\frac{\partial S}{\partial \phi}\right). \tag{15}$$

The energy balance equation at the solid–liquid interface is transformed to

$$\frac{\partial S}{\partial F_0} = -Ste\left(1 + \left(\frac{1}{\pi S}\frac{\partial S}{\partial \phi}\right)^2\right)\frac{\partial \eta}{\partial r}\frac{\partial \theta}{\partial \eta} \tag{16}$$

and the boundary conditions in the transformed domain are

$$\eta = 0; \quad \theta = 1, \quad \psi = \frac{\partial \psi}{\partial \eta} = 0 \tag{17}$$

$$\eta = 1; \quad \theta = 0, \quad \psi = \frac{\partial \psi}{\partial \eta} = 0 \tag{18}$$

$$\phi = 0 \quad \text{or} \quad 1; \frac{\partial \theta}{\partial \phi} = \psi = \omega = 0. \tag{19}$$

SOLUTION METHODOLOGY

A finite-difference method was used to obtain a numerical solution for the coupled governing equations (8–16) together with the boundary conditions, equations (17–19). The finite-difference analogs of the governing equations are derived by using central difference approximation in spatial derivatives and forward difference approximation in time derivatives except the convective terms for which the hybrid central/upwind difference scheme [11] is employed. The alternating directional implicit (ADI) splitting scheme [12] is adopted to formulate the resulting set of algebraic finite-difference equations in the convenient tridiagonal form. Then the solution of the set of difference equations can be efficiently obtained by using Thomas algorithm [13]. Moreover, the cross-differential terms in the governing equations are evaluated explicitly from the values of the variables at the previous time step.

The computational algorithm used in the present simulation is based on the solution procedure outlined by Ho and Viskanta [14, 15]. For all cases under consideration in the present study a grid system of 31 in the η-direction by 21 in the ϕ-direction was used.

RESULTS AND DISCUSSION

Numerical simulations of the melting of ice around an isothermal horizontal cylinder have been conducted for the cylinder surface temperature $T_i = 4$, 6, 8, 9, 10°C with cylinder radius $r_i = 25.4$ mm.

Flow pattern

Typical predicted streamlines and temperature distribution in the water during the melting process of ice are illustrated through a sequence of contour plots. In these plots, the inner dash–dot line circle designates the cylinder surface and the outer dash–dot line contour denotes the instantaneous solid–liquid interface profile. Figure 2 displays the evolution of the flow pattern and temperature distribution for the case $T_i = 4$°C ($Ste = 0.051$). In the early stage of the melting process, $F_0 = 0.7$, the heat conduction as expected is the dominant energy transport mechanism in the water as clearly indicated by the concentric isotherm distribution with a weak flow field in the narrow melt layer. As the melting continues, the convective motion in the water starts intensifying as evidenced by the downward shifting of the vortex center to the bottom as well as by the deformed isotherms. In this surface condition of $T_i = 4$°C, the water formed by melting near the cylinder is at a higher density than that near the ice interface; thus water near the surface of the cylinder moves downward while the relatively lighter water near the ice interface moves upward. Obviously, this recirculation behavior is opposite to that of normal fluids. At $F_0 = 3.2$ it appears that thermal boundary layers have been developed along the ice interface and the surface of the heated cylinder, respectively. Moreover, a thermal plume originates at the bottom portion of the ice interface. Consequently, the progress of the ice front in the bottom region is greatly enhanced. On the other end, the melting in the top region is markedly retarded. As time further proceeds the downward accelerating melting continues and an upside-down pear melt shape is clearly formed. Besides the reverse flow motion in the water due to its density anomaly, the characteristics of the flow pattern and melt shape are similar to those known for ordinary fluids [1–4].

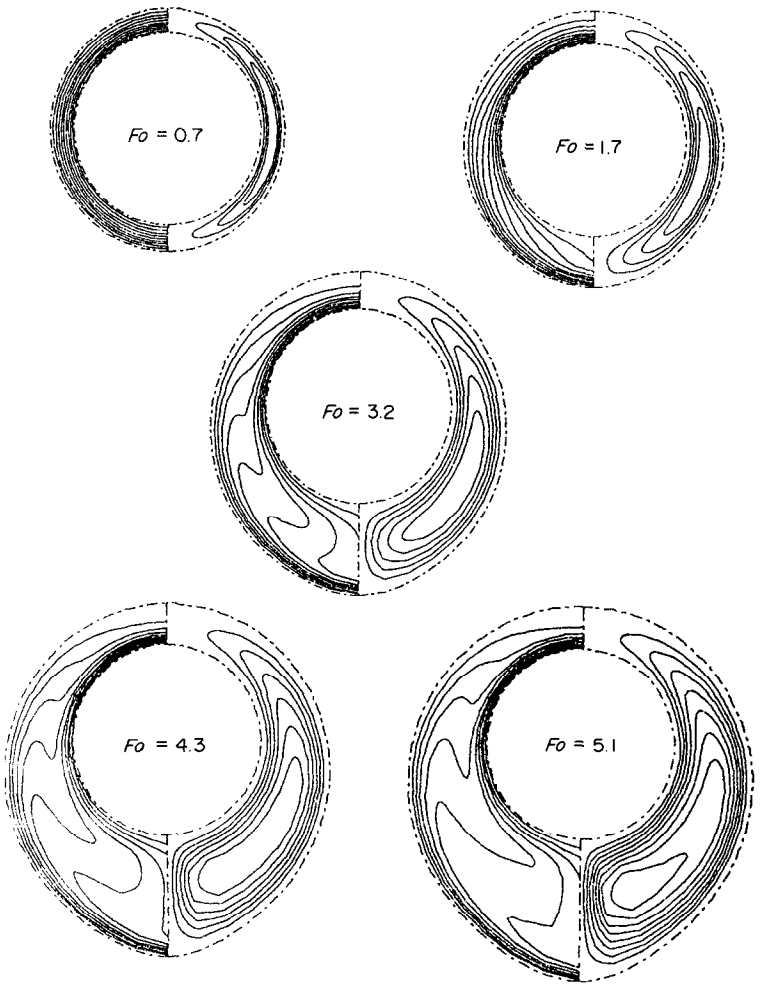

FIG. 2. Predicted distribution of isotherms (left) and streamlines (right) at various time for $T_i = 4$°C and $Ste = 0.56$.

In Fig. 3, the flow pattern and isotherm distributions at four different instants of time for $T_i = 8°C$ ($Ste = 0.101$) are shown. Due to the fact that the density of water at the ice interface and at the cylinder surface are approximately the same, the water with maximum density located somewhere in between moves downward and hence two counter-rotating circulating flows occur in the melt zone. As the melting proceeds, the outer circulation along the ice interface relatively intensifies and encompasses larger portion of the melt zone. As a result, the ice front movement is primarily determined by the outer circulation and a downward melting pattern appears. Besides, in the upper part of the melt zone, the melting process is noticeably retarded due to the circulation of cold melt in the region, as evidenced by the isotherm distribution in the figure.

Melting at $T_i = 10°C$ ($Ste = 0.126$), Fig. 4 shows that at the the early stage of melting, $F_0 = 0.3$, in the vicinity of the heat source a circulation moving upward along the cylinder surface is developed. Latter $F_0 = 0.8$, the vortex center of the circulation is shifting upward to the top region of the melt zone and hence a greatly enhanced melting occurs at the very top region above the heat source. A pear-like melt shape has already been formed at this early stage of the process. As the melting further progresses, a weaker counter vortex develops gradually in the melt front movement both at the top and the bottom of the cylinder. Furthermore, this outer circulation tends to limit the impinging range of the thermal plume arising from the top of heat source, resulting in a "bottleneck" melt shape. Such flow pattern is similar to that of natural convection of water encompassing density inversion without phase change in a horizontal cylindrical annulus [16].

A qualitative comparison between the predicted flow pattern of the present study and the flow visualization photographs of White [9], provided kindly by Prof. R. Viskanta of Purdue University, has been attempted and is shown in Fig. 5. Although the predicted flow pattern and the given flow visualization photographs are not at identical instants of time, a qualitative comparison can still be inferred. It is clearly indicated that in general the agreement in flow patterns is very good. It should be noted that White [9] also observed a three-dimensional vortex motion developed in the late stage of melting process, which apparently can not be predicted from the assumed two-dimensional numerical simulation of the present investigation.

Melt shape and melt volume

Figure 6 displays the transient progression of the interface contour for various heat source temperature. The aforementioned evolution of natural convection flow patterns in the molten water can be further inferred from the figure. Examination of the figure reveals that only at the early stage can a dominant role of conduction be deduced from the concentric melt shape for all cases. As soon as the melt layer thickness becomes large enough for the development of natural

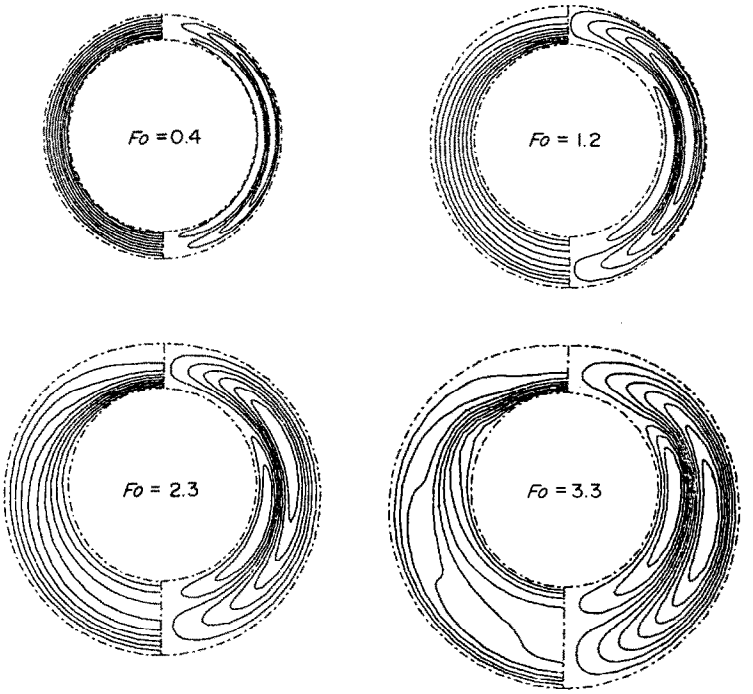

FIG. 3. Predicted distribution of isotherms (left) and streamlines (right) at various time for $T_i = 8°C$ and $Ste = 0.101$.

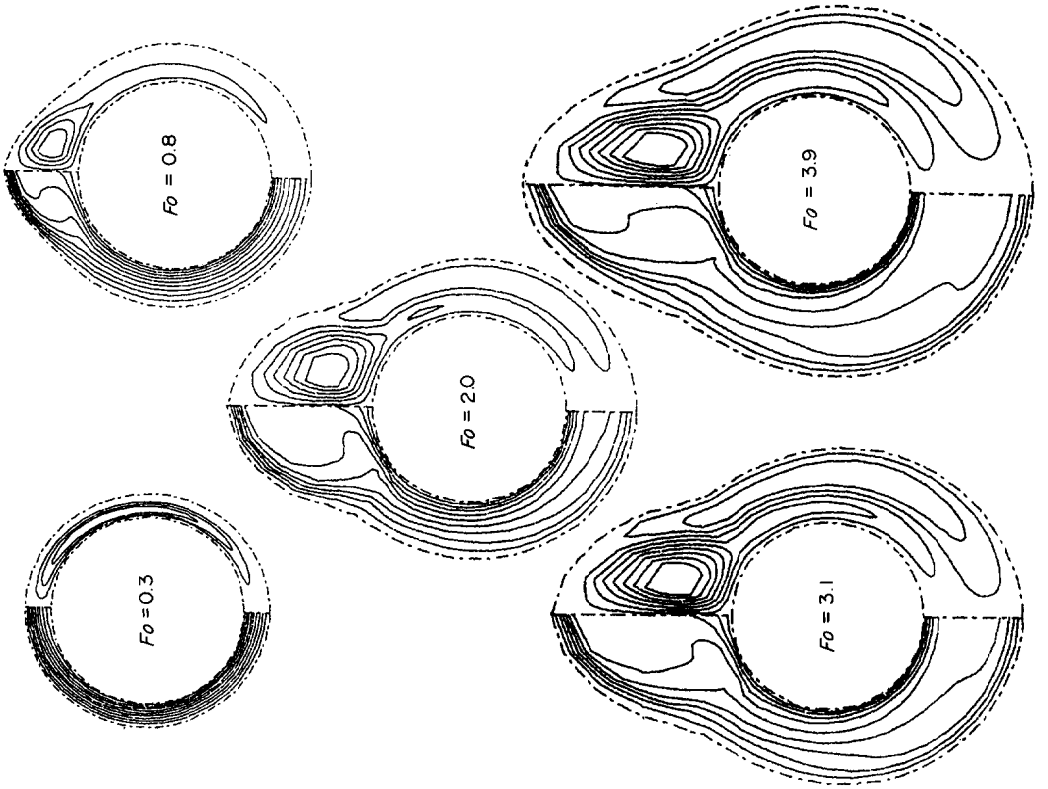

Fig. 4. Predicted distribution of isotherms (left) and streamlines (right) at various time for $T_i = 10°C$ and $Ste = 0.126$.

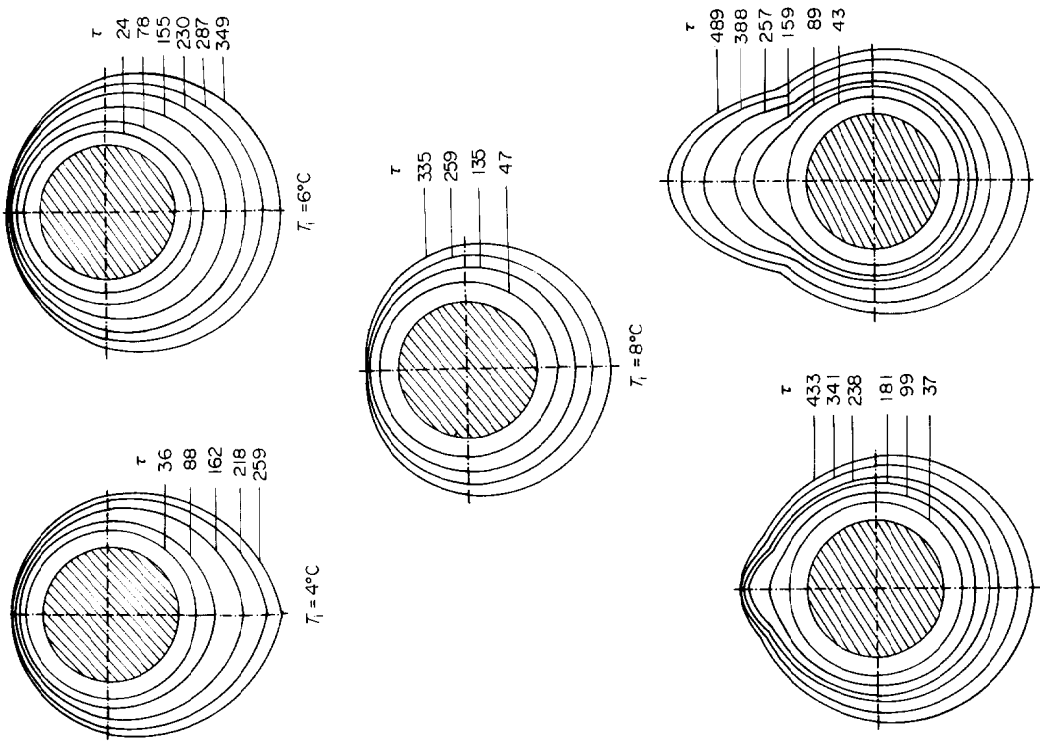

Fig. 5. Comparison of the predicted flow patterns with the experimental results by White [9].

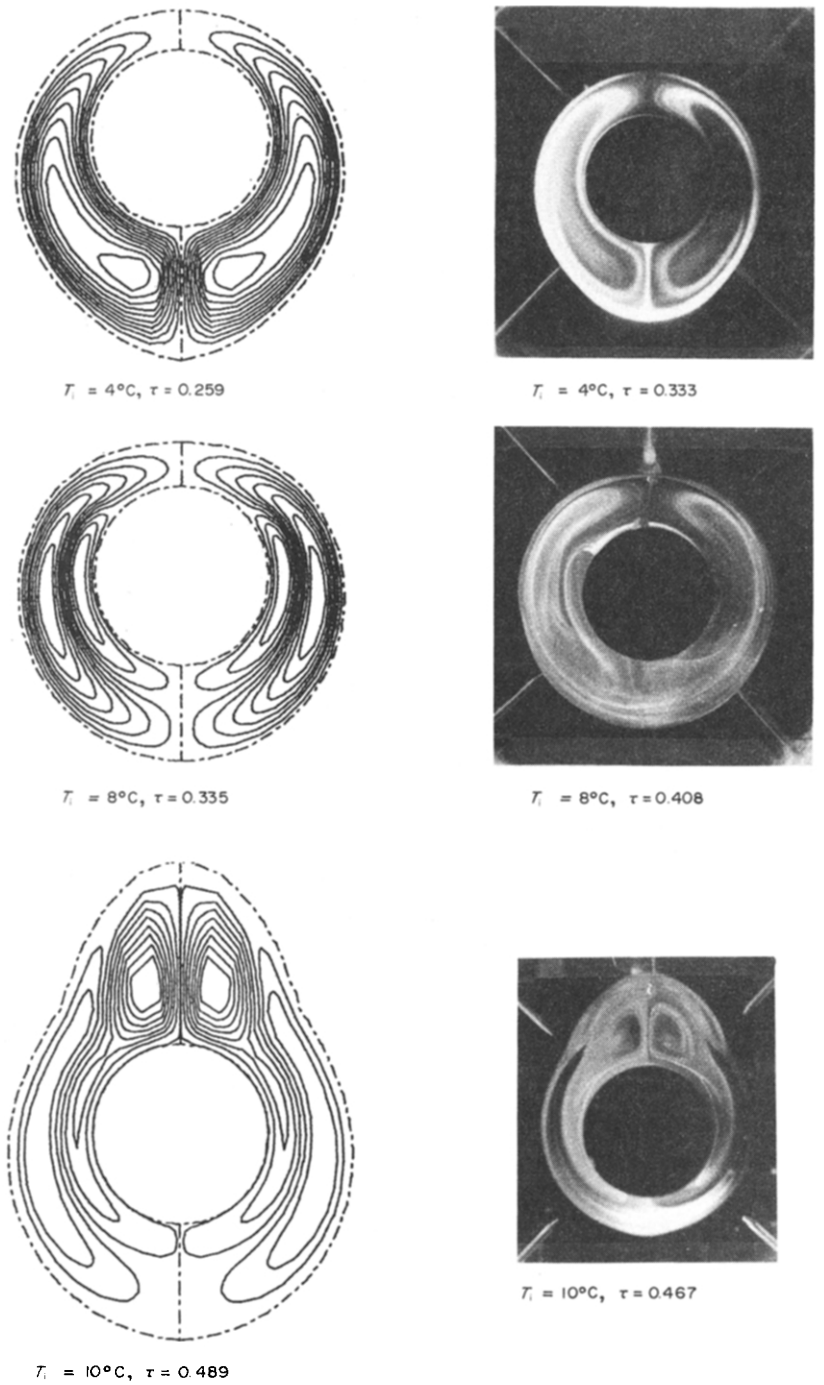

FIG. 6. The timewise melting front contours for various cylinder temperatures (dimensionless time $\tau \times 10^3$ as parameter).

convection of the melt, the melt shape evolves into different irregular contour depending on the development of the convective motion in the melt. For $T_i < 8°C$ ($Ste < 0.101$) natural convection develops mainly in the lower portion of the melt zone resulting in an upside-down pear melt shape; while for $T_i > 8°C$ ($Ste > 0.101$) the melting fronts propagate somewhat differently resulting from the interaction of the inner and outer circulation developed in the water zone. In particular, the melt shape at $T_i = 10°C$ ($Ste = 0.126$) resembles an upright pear due to the development of upward recirculation around the heat source.

The instantaneous molten volume ratio, V^*, is evaluated by a numerical integration of the instantaneous melting front contours and is defined as

$$V^* = \frac{V - V_0}{V_0} = \int_0^1 (S^2 - 1)\, d\phi, \qquad (20)$$

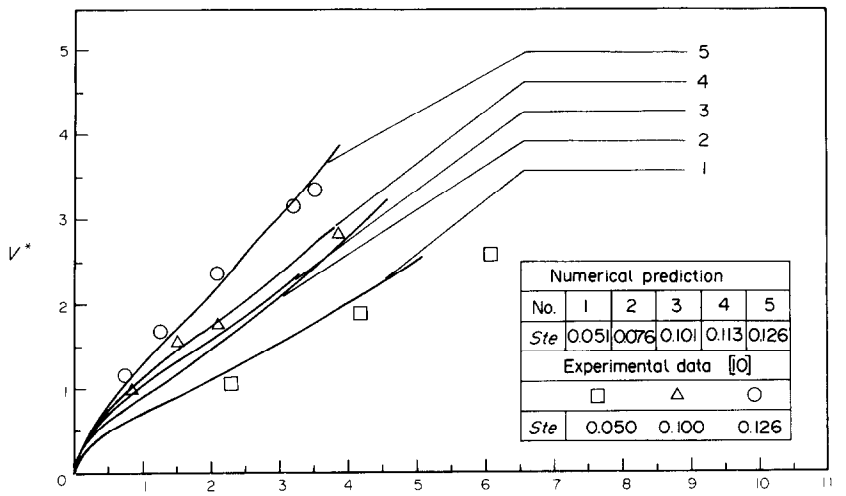

FIG. 7. Variation of melt volume ratio with Fourier number.

where V_0 is the volume of the heat source and V is the integrated volume of the melting front contour. The variation of V^* with dimensionless time F_0 for various Stefan numbers is depicted in Fig. 7. As expected, the molten volume increases with time as well as the Stefan number (or the heat source temperature). Experimental data of White [9] are also included in the figure to make a comparison with the prediction of the present simulation. It can be seen clearly from the figure that the agreement between the predictions and experimental data is reasonably good.

Heat transfer results

Attention is now turned to the heat transfer results during the melting process. The local heat transfer rates along the heat source surface as well as the ice interface can be expressed in terms of local Nusselt number Nu_i and Nu_s defined by

$$Nu_i \equiv -\frac{\partial \eta}{\partial r}\frac{\partial \theta}{\partial \eta} \tag{21}$$

$$Nu_s \equiv -\left(1+\left(\frac{1}{\pi S}\frac{\partial S}{\partial \phi}\right)^2\right)^{1/2}\frac{\partial \eta}{\partial r}\frac{\partial \theta}{\partial \eta}. \tag{22}$$

Figure 8 displays the variation of the local Nusselt numbers Nu_i and Nu_s with the dimensionless time τ for $T_i = 4°C$. Initial high values of both local Nusselt numbers with a sharp decline is a typical characteristic for transient one-dimensional conduction heat transfer. Such a conduction-dominated variation trend is ended by a spanwise spreading into individual curves for different angular locations. The local Nusselt number at the heat source surface displays a minimum and then rises smoothly in the following melting process. At the ice interface the variation history is somewhat different. For the lower portion of the interface, $\phi^+ < 72°$, the local Nusselt number passes a maximum following the initial declination to a minimum; while a monotonic decrease trend appears for the upper part of the interface. Similar timewise variation of the local heat transfer coefficients was also obtained by Rieger *et al.* [7] for melting of paraffin around a horizontal heat source. This is due to that at $T_i = 4°C$ the melted water does not encompass density inversion in between. As for the other situations under consideration, in the presence of changing complex natural circulation patterns developed in the molten water, rather complicated variations of the local heat transfer coefficients at both the heat source surface and the ice interface result. For instance, Fig. 9 shows the complicated trend of timewise vari-

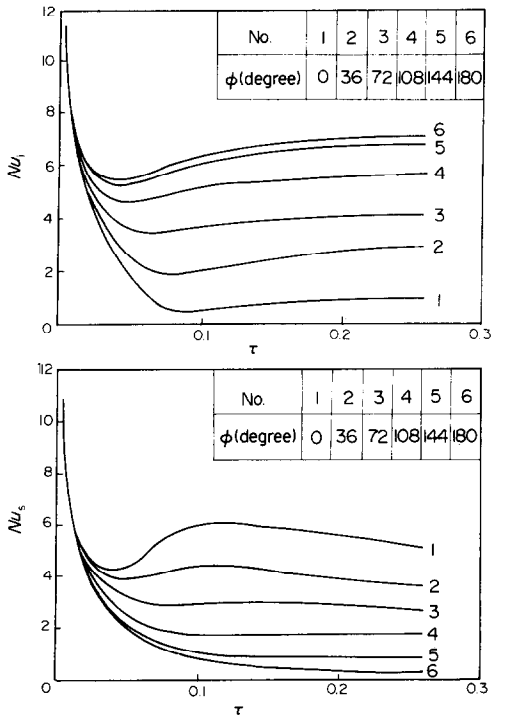

FIG. 8. Variation of the local heat transfer coefficients with dimensionless time for $T_i = 4°C$, $Ste = 0.056$.

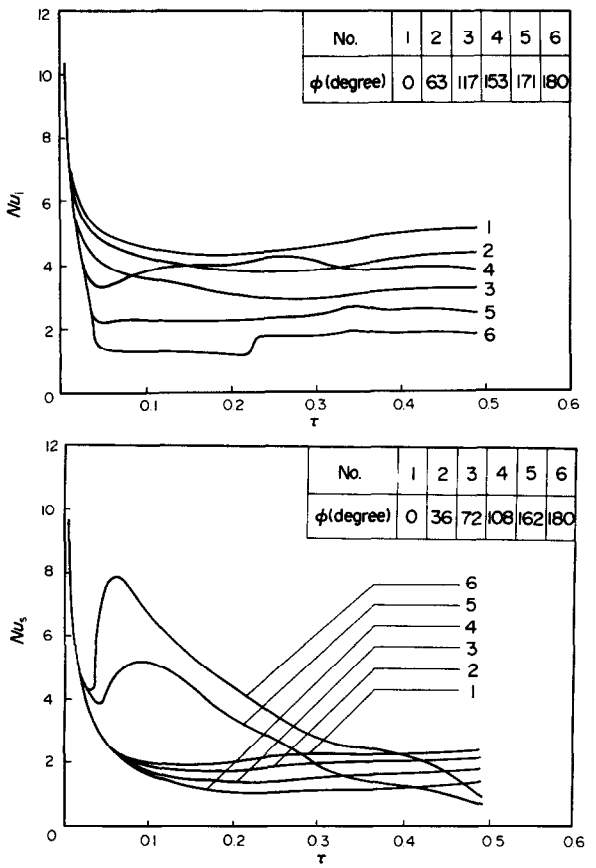

FIG. 9. Variation of the local heat transfer coefficients with dimensionless time for $T_i = 10°C$, $Ste = 0.101$.

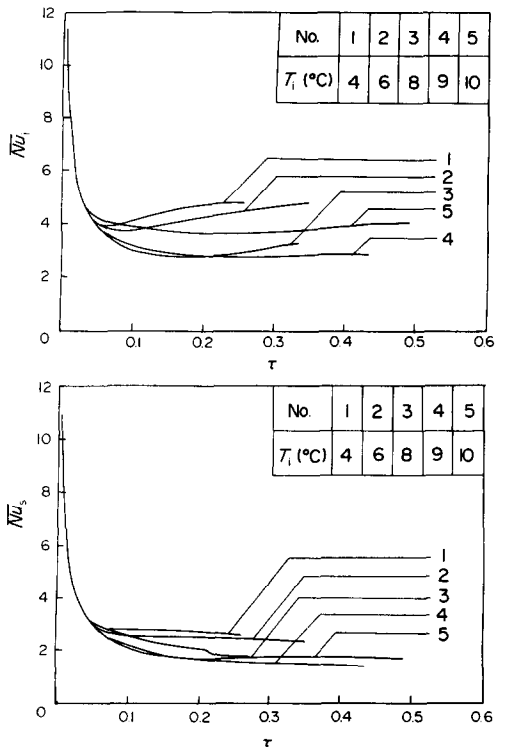

FIG. 10. Variation of the average heat transfer coefficients with dimensionless time for various cylinder temperatures.

ation of the local heat transfer coefficients for $T_i = 10°C$.

The average heat transfer coefficient at both the heat source surface and the ice interface is plotted vs the dimensionless time for various heat source temperature and is shown in Fig. 10. Following an initial sharp decline, the average heat transfer coefficient at the heat source surface passes a minimum and then rises smoothly. On the other hand, a monotonic decreasing trend with time appears for the average Nusselt number at the ice interface, except for the case of $T_i = 8°C$. Further examination of the figure indicates that for $\tau < 0.2$, both average heat transfer coefficients for $T_i = 8°C$ appear to be the smallest among the cases considered, and surpass that for $T_i = 9°C$ in the remaining melting process. This result clearly indicates that the minimum heat transfer rate does not always occur for $T_i = 8°C$, which is apparently in contradiction to the postulation made by Herrmann that the minimum heat transfer occurs at $T_i = 8°C$. However, it should be noted that the experimental results by Herrmann do not include any case for $T_i = 9°C$ and thus it remains open to further studies concerning such uncertainty.

CONCLUDING REMARKS

Numerical simulation has been performed for outward melting of ice around a horizontal isothermal

cylinder. Results clearly indicate that the melting process of ice around a horizontal cylinder is strongly affected by the changing recirculation flow developed in the molten water, which, due to the density anomaly of the water in the temperature range under consideration, is more complex than those during the similar melting process of normal phase change material. A comparison of the predicted flow patterns with the flow visualization results by White appears to be in good agreement. For $T_i < 8°C$ ($Ste < 0.101$) an upside-down pear like melt shape occurs; while for $T_i > 8°C$ ($Ste > 0.101$) an upright pear like melt shape appears. Also, the predicted melt volume is in reasonably good agreement with the results by White. The heat transfer results reveal that the minimum average heat transfer does not always occur for $T_i = 8°C$ as postulated by Herrmann *et al.* Instead, during the latter stage of melting process, $T_i = 9°C$ appears to be the one with the minimum average heat transfer. Further experimental exploration is apparently needed to clarify such uncertainty.

Acknowledgement—The authors wish to express their sincere thanks to Prof. Raymond Viskanta and Mr. David A. White for kindly providing the experimental results and flow visualization photographs of their work on the similar problem.

REFERENCES

1. A. G. Bathelt, R. Viskanta and W. Leindenfrost, An experimental investigation of natural convection in the melted region around a heated horizontal cylinder, *J. Fluid Mech.* **90,** 227–239 (1979).
2. E. M. Sparrow, R. R. Schmidt and J. W. Ramsey, Experiments on the role of natural convection in the melting of solids, *J. Heat Transfer* **100,** 11–16 (1978).
3. R. M. Abdel-Washed, J. M. Ramsey and E. M. Sparrow, Photographic study of melting about an embedded horizontal heating cylinder, *Int. J. Heat Mass Transfer* **23,** 171–173 (1979).
4. A. G. Bathelt and R. Viskanta, Heat transfer at the solid–liquid interface during melting from a horizontal cylinder, *Int. J. Heat Mass Transfer* **23,** 1493–1503 (1980).
5. R. Viskanta, *Phase-Change Heat Transfer in Solar Heat Storage: Latent Heat Materials* (edited by G. A. Lane), Vol. 1, pp. 153–222. CRC Press, Boca Raton, Florida (1983).
6. L. S. Yao and F. F. Chen, Effects of natural convection in the melted region around a heated horizontal cylinder, *J. Heat Transfer* **102,** 667–673 (1980).
7. H. Rieger, U. Projahn and H. Beer, Analysis of the heat transport mechanism during melting around a horizontal circular cylinder, *Int. J. Heat Mass Transfer* **25,** 137–147 (1982).
8. J. Herrmann, W. Leindenfrost and R. Viskanta, Melting of ice around a horizontal isothermal cylindrical heat source, *Chem. Engr. Commun.* **25,** 63–78 (1984).
9. D. A. White, Melting of ice and freezing of water around a horizontal cylinder, M.S. Thesis, Purdue University, W. Lafayette, Indiana (1984).
10. B. Gebhart and J. Mollendorf, A new density relation for pure and saline water, *Deep-Sea Research* **124,** 831–848 (1977).
11. S. V. Patankar, *Numerical Heat Transfer and Fluid Flow.* Hemisphere, McGraw-Hill, New York (1980).
12. R. Peyret and T. D. Taylor, *Computational Methods for Fluid Flow.* Springer, New York (1983).
13. P. J. Roache, *Computational Fluid Dynamics.* Hermosa, Albuquerque, New Mexico (1976).
14. C. J. Ho and R. Viskanta, Heat transfer during melting from an isothermal vertical wall, *J. Heat Transfer* **106,** 12–19 (1984).
15. C. J. Ho and R. Viskanta, Heat transfer during melting in a horizontal tube, *Int. J. Heat Mass Transfer* **27,** 705–716 (1984).
16. P. Vasseur, L. Robillard and B. C. Shekar, Natural convection heat transfer of water within a horizontal cylindrical annulus with density inversion effect, *J. Heat Transfer* **105,** 117–123 (1983).

SIMULATION NUMERIQUE DE LA FUSION DE LA GLACE AUTOUR D'UN CYLINDRE HORIZONTAL

Résumé—Le problème de la fusion externe de la glace autour d'un cylindre horizontal isotherme est considéré. On développe un modèle numérique dans lequel la convection naturelle induite dans l'eau de fusion avec inversion de densité est prise en compte. Par une résolution aux différences finies, on obtient la simulation numérique de la fusion de la glace pour une température de la surface du cylindre $T_i = 4$, 6, 8, 9 et 10°C et un rayon du cylindre égal à 25,4 mm. Les résultats de cette simulation sont quantitativement admissibles en comparaison avec les données expérimentales connues.

NUMERISCHE SIMULATION DES SCHMELZENS VON EIS AN EINEM WAAGERECHTEN ZYLINDER

Zusammenfassung—Der Fall des Schmelzens von Eis an der Außenseite eines waagerechten isothermen Zylinders wird betrachtet. Es wurde ein numerisches Modell entwickelt, das die natürliche Konvektion im geschmolzenen Wasser unter Berücksichtigung des Dichtemaximums enthält. Mit Hilfe eines Differenzenverfahrens wurde das Modell des Schmelzvorgangs gelöst, die numerische Simulation des Schmelzvorgangs wurde für Oberflächentemperaturen des Zylinders von $T_i = 4°$, 6°, 8°, 9° und 10°C bei einem Zylinderradius von 25,4 mm durchgeführt. Es stellte sich eine qualitative Übereinstimmung zwischen der Simulation und vorhandenen Versuchsergebnissen heraus.

ЧИСЛЕННОЕ МОДЕЛИРОВАНИЕ ПЛАВЛЕНИЯ ЛЬДА ВОКРУГ ГОРИЗОНТАЛЬНОГО ЦИЛИНДРА

Аннотация—Рассматривается задача наружного плавления льда вокруг горизонтального изотермического цилиндра. Разработана численная модель, в которой рассматривается естественная конвекция в воде, возникшей в результате плавления льда, с учетом инверсии плотности. Плавление льда исследуется численно с помощью конечно-разностного метода при температурах поверхности цилиндра $T_i = 4°$, $6°$, $8°$, $9°$ и $10°C$ и при радиусе цилиндра, равном 25,4 мм. Сравнение результатов данного моделирования с существующими экспериментальными данными показало их качественное совпадение.